PERGAMON

Continental Shelf Research 22 (2002) 1821–1833

CONTINENTAL SHELF RESEARCH

www.elsevier.com/locate/csr

The effect of geometry and bottom friction on local bed forms in a tidal embayment

G.P. Schramkowski*, H.M. Schuttelaars[1], H.E. de Swart

Institute for Marine and Atmospheric Research Utrecht, Utrecht University, Princetonplein 5, 3508 TA Utrecht, The Netherlands

Abstract

Using a 2DH idealized local morphodynamic model for a tidal channel, it is demonstrated that estuarine bars with typical length scales on the order of the tidal excursion length can develop as the result of a positive feedback between water motion, sediment transport and the sandy bottom. The water motion is modelled by the depth-averaged shallow water equations and driven by an externally prescribed M_2 tide. Sediment is mainly transported as suspended load due to advective processes. Convergences and divergences of the tidally averaged sediment fluxes result in the evolution of the bed. It is shown that the combined effect of bottom friction and advective processes can trigger instabilities that lead to the formation of bottom patterns. Bed slope effects are required in order to prevent infinite braiding of these features. With bed slope effects, bars with longitudinal length scales of the order of the tidal excursion length are most likely to become unstable. This result is found to be independent of the ratio of the width to the tidal excursion length as well as the adopted formulation of the bed shear stress. In the case that the width is much smaller than the tidal excursion length and non-linear bottom friction is used, there is good qualitative agreement with results from 3D models reported in literature which were applied to the same parameter regime. Qualitatively, the results are recovered when bottom friction is linearized. Quantitatively, only small modifications occur: the critical friction parameter is decreased and the longitudinal length scale of the most unstable bed form increases.

Keywords: Bed forms; Tides; Estuaries; Estuarine dynamics; Mathematical models; Suspended load

1. Introduction

The geomorphology of semi-enclosed tidal embayments with a sandy bed often consists of a complex network of channels and shoals. In the channels, strong tidal currents are observed (of order 1 m s^{-1}). Field data indicate that different types of bed forms can exist. On the one hand, near the entrance of shallow embayments (e.g. those located along the east coast of the United States) the so-called estuarine bars are often observed (Dalrymple and Rhodes, 1995). These rhythmic bars have wavelengths which are related to the embayment width and do not migrate. On the other hand, deeper embayments, e.g. those located in the Dutch and German Wadden Sea, are characterized by a fractal pattern of channels (cf. Cleveringa and Oost, 1999; Ehlers, 1988) which appear to scale with the length of the embayment. Often both types of bottom patterns can be observed simultaneously. An example is the Western Scheldt, a tidal estuary located at the

*Corresponding author. Fax: +31-30-254-3163.
E-mail address: g.p.schramkowski@phys.uu.nl (G.P. Schramkowski).
[1]Also at Delft University of Technology, Stevinweg 1, 2628 CN Delft, The Netherlands.

0278-4343/02/$ - see front matter
PII: S0278-4343(02)00040-7

Dutch–Belgium border. Its marine part has a length of about 90 km and can be divided into six separate sections. Within these sections, bars are observed which are related to the embayment width, see Jeuken (2000); Van den Berg et al. (1997).

Knowledge about the behaviour of these bar–shoal systems is relevant, both for estuarine management and scientific purposes. For example, the morphology influences ship routing, but it also plays an important role in determining the flushing characteristics of the water motion and thereby the ecological diversity of the area (Verbeek et al., 1999). In semi-empirical models, see e.g. Di Silvio (1989); Van Dongeren and de Vriend (1994), the shoal surface area is often parametrically accounted for. From a process-oriented perspective the evolution of bars has been successfully simulated by Wang et al. (1995) and Ranasinghe et al. (1999). These models are rather complex and have not been designed to gain fundamental understanding about the physical mechanisms controlling the channel–shoal dynamics. For the latter objective idealized models, which focus on isolated processes, are useful tools.

It has been demonstrated by Seminara and Tubino (1998) and Schuttelaars and De Swart (1999) that bars in tidal channels can form as inherent morphologic instabilities. Seminara and Tubino (1998) analyse a local model, which in general is designed to deal with phenomena that scale on a length scale which is small compared with both the tidal wavelength and channel length. In this approach the water motion must be prescribed by specifying external pressure gradients which result from the dynamics on the global scale. In their study Seminara and Tubino (1998) use a three-dimensional model, based on the shallow water equations. They also a priori assume that the embayment width is the controlling length scale of the bed forms. Their model results apply to narrow, frictionally dominated tidal channels.

Schuttelaars and De Swart (1999) on the other hand study a global model of a semi-enclosed tidal basin where the water motion is driven by a prescribed vertical tide at the seaward boundary. This choice implies that they put emphasis on bottom patterns that occur on the length scale of the entire domain. Their model is based on the depth-averaged shallow water equations and assumes that the ratio of the tidal excursion length and the embayment length is small. Results are presented for the case of a short embayment (with a length being much smaller than the tidal wavelength), in which sediment transport is dominated by diffusive processes and advective terms in the flow and sediment equations can be neglected. However, the model can be generalized in a straightforward sense, as is demonstrated in Schuttelaars and De Swart (2000) (1D equilibrium dynamics in a long embayment) and in Van Leeuwen and De Swart (2001) (2D non-linear bed forms in a short embayment).

Thus, global and local models may be viewed as describing morphodynamics for opposite limits with regard to the length scales of bottom patterns. The results from the two approaches should qualitatively agree in the appropriate limits. This is not straightforward, because the local model of Seminara and Tubino (1998) and the non-linear global model of Schuttelaars and De Swart (2000) use different formulations and assumptions. This motivates the set up of an intermediate model, in which both the embayment width and the tidal excursion length are retained as relevant length scales. Hence, this model can deal with phenomena that scale on a length scale which is small compared with both the tidal wavelength and embayment length, but not necessarily small compared with the tidal excursion length. Moreover, in the intermediate model discussed in this paper the ratio of the frictional timescale and tidal period can be arbitrarily varied, which is an important generalisation with respect to the model of Seminara and Tubino (1998). This intermediate model serves as a link between the two models which are already available. Here, the intermediate model will be compared with the results by Seminara and Tubino (1998). It will be shown that in the limit of a narrow and frictionally dominated channel, the bed forms found by the latter authors will be recovered. In a forthcoming paper, the connection with the bed forms found in a global model (see Schuttelaars et al., 2001) will be made.

The paper is organized as follows. In Section 2 the local model is described. In Section 3 the

method of analysis that is used to describe the formation of bed forms is described. In Section 4 the results from the local analysis will be presented. Finally, the results will be discussed in Section 5.

2. Model description

The features studied in this paper have length scales which are small compared with the tidal wavelength, the embayment length and the length scale on which variations of the channel width occur. On the other hand, their length scales are large with respect to the water depth. Hence, the geometry of the model is represented as an infinitely long channel having a constant width B. The banks are straight and non-erodible, with only the bottom being subject to erosion (see Fig. 1). The total water depth is denoted by $D = H - h$ where H is a reference depth, while $u(x)$ and $v(y)$ are the along-channel and cross-channel velocities (coordinates), respectively.

The model is forced by a prescribed external tide. This explicitly reflects the local nature of the model which *by definition* cannot solve the global tidal motion self-consistently. It will be assumed that the external tide contains only an M_2 component.

The water motion is described by the depth-averaged shallow water equations (see Vreugdenhil, 1994). Within the local model, tidal velocities are of the order of 1 m s^{-1}. Since the amplitude of the sea surface elevations is assumed to be much smaller than the undisturbed water depth, the so-called rigid lid approximation can be adopted. This implies that the water level ζ and its derivatives may be neglected everywhere except for terms that describe tidal forcing, i.e. $g\zeta_x$ and $g\zeta_y$. These latter terms describe, for instance, the forcing due to the prescribed external tide. Furthermore, since the bed changes on a timescale that is long compared to the tidal period, the bottom can be considered time independent on the short tidal timescale. The resulting equations read

$$(Du)_x + (Dv)_y = 0, \tag{1a}$$

$$u_t + uu_x + vu_y + F_1^{\mathrm{b}} = -g\zeta_x, \tag{1b}$$

$$v_t + uv_x + vv_y + F_2^{\mathrm{b}} = -g\zeta_y, \tag{1c}$$

where subscripts denote differentiation, g is the gravitational acceleration and $\boldsymbol{F}^{\mathrm{b}} = (F_1^{\mathrm{b}}, F_2^{\mathrm{b}})$ the bottom friction. The friction vector is defined as

$$\boldsymbol{F}^{\mathrm{b}} = \frac{\boldsymbol{\tau}^{\mathrm{b}}}{\rho(H-h)}, \tag{2}$$

with $\boldsymbol{\tau}^{\mathrm{b}}$ the bed shear stress vector, which is in general a non-linear function of velocity. Using a procedure first proposed by Lorentz (1922), see also Zimmerman (1992), the non-linear bottom friction can be linearized in such a way that averaged over one tidal cycle the same amount of energy is dissipated in both formulations. Since linearized bottom friction gives the same qualitative results as the non-linear formulation, while it is easier to analyse, we will hereafter use the linearized shear stress unless stated otherwise. Hence,

$$\boldsymbol{\tau}^{\mathrm{b}} = \rho r \boldsymbol{u},$$

where r is a friction parameter with dimensions m s^{-1}.

The impermeability of side walls to water motion implies that the cross-channel velocity v should vanish at the banks, i.e.

$$v = 0 \quad \text{at } y = 0, B. \tag{3}$$

The bed of the estuaries considered consists of fine non-cohesive sediment (typical grain size of

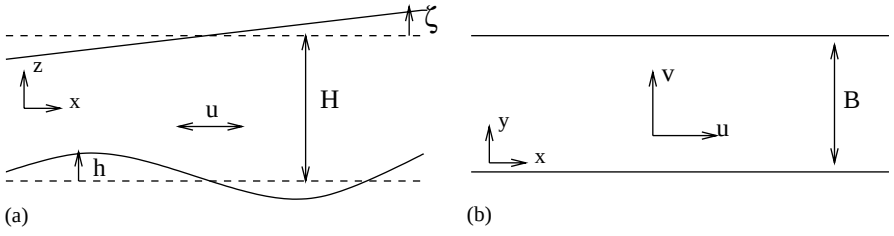

Fig. 1. The side view (a) and top view (b) of the embayment. For an explanation, see the text.

2×10^{-4} m) which is mainly transported as suspended load. The dynamics of the suspended sediment is described by an advection–diffusion equation for the so-called *volumetric* depth-integrated concentration C (with dimension m), which is defined as the depth-integrated sediment concentration divided by the sediment density. The evolution equation for C reads (Van Rijn, 1993)

$$C_t + (uC - \mu C_x)_x + (vC - \mu C_y)_y = S \equiv \alpha(u^2 + v^2) - \gamma C, \quad (4)$$

where μ denotes the horizontal coefficient for sediment diffusion and S the difference between erosion and sedimentation at the top of the active layer. Typically, $\mu = \mathcal{O}(10-100)$ m^2 s^{-1} for tidal flows in estuaries. The first term on the right-hand side of Eq. (4) models the sediment pick-up function, and the second term the tendency of sediment to settle due to gravity effects. The adopted values of the coefficients α ($\mathcal{O}(10^{-5}-10^{-7})$ s m^{-1}) and γ ($\mathcal{O}(10^{-3}-10^{-2})$ s^{-1}) are representative for fine sand (see e.g. also Dyer, 1986).

The non-erodibility of the banks implies that there is no sediment flux through the side walls, i.e.

$$vC - \mu C_y = 0 \quad \text{at } y = 0, B. \quad (5)$$

The evolution of the bottom follows from the conservation of sediment. Since the bed in general evolves on a timescale (typically weeks to months) which is long compared to a tidal period, the dynamics of bottom patterns is not sensitive to instantaneous rates of erosion and deposition, but rather to their tidal mean values. The resulting equation for the bottom evolution thus reads

$$h_t + \langle \nabla \cdot \boldsymbol{S}_b \rangle = -\langle S \rangle, \quad (6)$$

where $\langle\ \rangle$ denotes the time average over an M_2 tidal period. The sedimentation function S is defined in Eq. (4). The volumetric bed-load sediment flux in the active layer is denoted by $\boldsymbol{S}_b$ and parameterized as Engelund (1975)

$$\boldsymbol{S}_b = \hat{s}\|\boldsymbol{u}\|^b \left(\frac{\boldsymbol{u}}{\|\boldsymbol{u}\|} - \kappa_\star \nabla h \right).$$

Typical values for b, $\kappa_\star$ and $\hat{s}$ are $b \sim 3$, $\kappa_\star \sim 2$ and $\hat{s} \sim 3 \times 10^{-4}$ s^2 m^{-1} while it is assumed that the critical shear stress is effectively zero in view of the strong tidal currents. In the situations under study, the fluxes associated with the bed-load transport $\boldsymbol{S}_b$ are much smaller than those related to the suspended-load transport S, typically by a factor of 0.1–0.01. This implies that bed-load transport is small compared to suspended-load transport and hence can be neglected. However, the bed slope correction term ($\propto \kappa_\star \nabla h$) cannot be ignored in case of bed forms with short spatial oscillations and has to be incorporated in the model. This seems to be consistent with literature where it is suggested that the transport due to the bed slope terms cannot be neglected (see Parker, 1978; Talmon et al., 1995), even if suspended-load transport dominates.

3. Linear stability analysis

For realistic values of the parameters the 2D system of equations, as described in Section 2, allows for a morphodynamic equilibrium solution $\boldsymbol{\Psi}_{eq} = (u, v, \nabla\zeta, C, h)_{eq}$, which is spatially uniform, i.e. they are independent of both the x- and the y-coordinate. In case that the forcing of the water motion (due to the externally prescribed pressure gradient) consists of one single tidal constituent (an M_2 component with frequency $\sigma = 1.4 \times 10^{-4}$ s^{-1}), it reads

$$\boldsymbol{\Psi}_{eq} = (U\cos(\sigma t), 0, \nabla\zeta_{eq}, C_{eq}, 0)$$

with

$$(\zeta_{eq})_x = \frac{\sigma U}{g}\left[\sin(\sigma t) - \frac{r}{\sigma H}\cos(\sigma t)\right], \quad (\zeta_{eq})_y = 0, \quad (7a)$$

$$C_{eq} = \frac{\alpha U^2}{2\gamma}\left[1 + \frac{\gamma^2\cos(2\sigma t) + 2\sigma\gamma\sin(2\sigma t)}{\gamma^2 + 4\sigma^2}\right]. \quad (7b)$$

This describes a tidal flow in a channel with an undisturbed water depth H and a horizontal bottom. The concentration consists of a residual component as well as of a component which oscillates with twice the basic tidal frequency. This equilibrium solution is in general not stable with respect to perturbations having a structure in the cross-channel direction. This means that such perturbations can grow due to a positive feedback between the water motion and the erodible bed.

The dynamics of the perturbations is analysed by substitution of

$$\boldsymbol{\Psi}(x,y,t) = \boldsymbol{\Psi}_{\mathrm{eq}}(t) + \boldsymbol{\Psi}'(x,y,t)$$

in the full equations of motion. Linearizing these equations with respect to the small perturbations results in

$$Hu'_x + Hv'_y = u_{\mathrm{eq}} h'_x, \tag{8a}$$

$$u'_t + u_{\mathrm{eq}} u'_x + F_1^{\mathrm{b}'} = -g\zeta'_x, \tag{8b}$$

$$v'_t + u_{\mathrm{eq}} v'_x + F_2^{\mathrm{b}'} = -g\zeta'_y, \tag{8c}$$

$$C'_t + u_{\mathrm{eq}} C'_x + (u'_x + v'_y) C_{\mathrm{eq}} + \mu\nabla^2 C' = 2\alpha u_{\mathrm{eq}} u' - \gamma C', \tag{8d}$$

$$h'_t - \lambda\nabla^2 h' = -\langle 2\alpha u_{\mathrm{eq}} u' - \gamma C' \rangle \tag{8e}$$

with $\lambda = \hat{s}\langle |\boldsymbol{u}_{\mathrm{eq}}|^b \rangle \kappa_\star \sim 10^{-4}$ m^2 s^{-1} and $\boldsymbol{F}^{\mathrm{b}'}$ the perturbed bottom friction vector. In the linearized context this vector reads

$$\boldsymbol{F}^{\mathrm{b}'} = \left(\frac{r}{H}u' + \frac{r u_{\mathrm{eq}}}{H^2}h', \frac{r}{H}v'\right).$$

Finally, we note that Eq. (8d) can be used to rewrite Eq. (8e) in the following form:

$$h'_t = -\nabla \cdot \langle \mathscr{F} \rangle, \tag{9}$$

where

$$\mathscr{F} = \mathscr{F}_{\mathrm{adv}} + \mathscr{F}_{\mathrm{diff}} + \mathscr{F}_{\mathrm{bed}}$$

with

$$\mathscr{F}_{\mathrm{adv}} = \boldsymbol{u}_{\mathrm{eq}} C' + \boldsymbol{u}' C_{\mathrm{eq}},$$
$$\mathscr{F}_{\mathrm{diff}} = -\mu\nabla C', \quad \mathscr{F}_{\mathrm{bed}} = -\lambda\nabla h'$$

denoting the advective, diffusive and bedslope contributions to the sediment flux, respectively. Here, $\boldsymbol{u}_{\mathrm{eq}} = (u_{\mathrm{eq}}, 0)$ and $\boldsymbol{u}' = (u', v')$ are the equilibrium and perturbed velocity vector. From Eq. (9) we see that the bed level rises (descends) when the total net sediment flux converges (diverges).

The structure of the linearized Eqs. (8) and the boundary conditions allow for solutions written as

$$(u', \zeta', C', h') = \Re[(\hat{u}(t), \hat{\zeta}(t), \hat{C}(t), \hat{h}(t)) \cos(l_n y) \mathrm{e}^{\mathrm{i}kx}], \tag{10a}$$

$$v' = \Re[\hat{v}(t) \sin(l_n y) \mathrm{e}^{\mathrm{i}kx}]. \tag{10b}$$

Here $l_n = n\pi/B$ where $n = 0, 1, 2, \ldots$ is the cross-channel mode number and k is an arbitrary longitudinal wavenumber. $\Re$ denotes the real part of the solution. Hereafter, $\hat{h}$ is assumed to be real: this may be done without loss of generality because the equilibrium state is spatially uniform.

The timescale associated with the evolution of the bed is much longer than the tidal timescale. The ratio of the tidal period and the morphologic timescale is typically of the order of 10^{-2}–10^{-4}. Since Eqs. (8a)–(8d) evolve on the tidal timescale, the bed perturbation h' in these equations can be considered fixed. Now the fast variables can be calculated for a given bed perturbation as a Fourier series:

$$\hat{u}(t), \hat{v}(t), \hat{\zeta}(t), \hat{C}(t)) = \hat{h} \sum_p (\tilde{u}, \tilde{v}, \tilde{\zeta}, \tilde{C}) \mathrm{e}^{\mathrm{i}p\sigma t}. \tag{11}$$

Substituting Eq. (10) in the bed evolution equation (8e), which is determined by the tidally averaged transport, results in

$$\partial_t \hat{h} = \omega \hat{h}, \tag{12}$$

where the eigenvalue ω reads

$$\omega = [-\mathrm{i}k\langle u_{\mathrm{eq}} \hat{C} \rangle - \langle (\mathrm{i}k\hat{u} + l_n \hat{v}) C_{\mathrm{eq}} \rangle - \mu(k^2 + l_n^2)\langle \hat{C} \rangle - \lambda(k^2 + l_n^2)\hat{h}]/\hat{h} \tag{13}$$

and $(\hat{u}(t), \hat{v}(t), \hat{\zeta}(t), \hat{C}(t))$ is defined in Eq. (11). The first two terms on the right-hand side of Eq. (13) give the contribution of the divergence of the advective sediment flux $\mathscr{F}_{\mathrm{adv}}$, while the last two terms model the divergences of fluxes due to diffusive processes ($\mathscr{F}_{\mathrm{diff}}$) and bedslope effects ($\mathscr{F}_{\mathrm{bed}}$), respectively. For a more detailed description of the method used, see e.g. Hulscher et al. (1993).

For given model parameters, the eigenvalue ω of the associated perturbation can be calculated for every mode number k and l_n. The real part of the eigenvalue $\Re(\omega)$ denotes the growth rate of the perturbation and $-\Im(\omega)/k$ its migration speed. If the growth rate is positive ($\Re(\omega) > 0$), the perturbation grows and the basic state is unstable. It turns out that if the system is only forced with an M_2 tide, the migration speed is always zero.

We will now give a more geometric interpretation of the advective contributions to Eq. (13). To

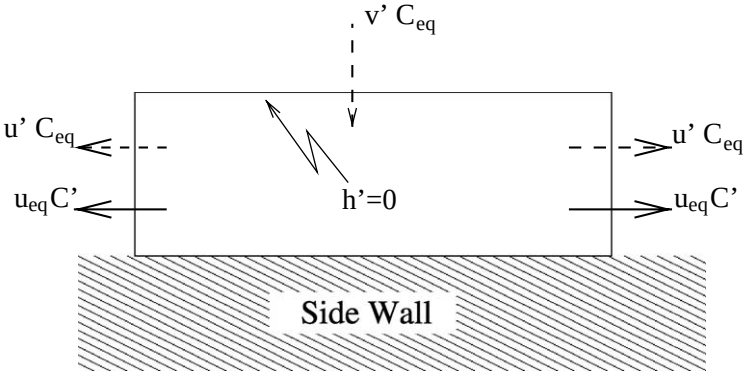

Fig. 2. The net advective sediment fluxes entering/leaving a region $\mathscr{D}$ which is on one side bounded by the sidewall and on the other sides by the line $h' = 0$.

this end, Fig. 2 shows the advective flux $\mathscr{F}_{\text{adv}}$ that enters/leaves the smallest possible region $\mathscr{D}$ bounded by the sidewall and a line with $h' = 0$. Such a region can always be found since $\Im(\omega) = 0$. Moreover, without loss of generality, it may henceforth be assumed that the region contains a crest ($h' > 0$) while it is bounded by $x = \pm\pi/(2k)$ and $y = 0,\ \pi/(2l_n)$. Indeed, when the bedform inside the region grows or decays, so will the bottom perturbation throughout the entire channel since the bedform is an eigenfunction (see Eq. (12)).

The net deposition or sedimentation due to the contribution $\boldsymbol{u}'C_{\text{eq}}$ to $\mathscr{F}_{\text{adv}}$ is zero. This can be seen as follows. Mass conservation (8a), with Eq. (10), gives $\mathrm{i}k\hat{u} + l_n\hat{v} = \mathrm{i}ku_{\text{eq}}\hat{h}/H$. It can then be easily seen that

$$(\mathrm{i}k\hat{u} + l_n\hat{v})C_{\text{eq}} = \mathrm{i}ku_{\text{eq}}C_{\text{eq}}\hat{h}/H. \tag{14}$$

Recalling that u_{eq} only has an M_2 component and C_{eq} has a residual component and a part that oscillates with twice the basic tidal frequency (see Eq. (7b)), it is clear that the tidal average of Eq. (14) is zero. In other words: $\langle \nabla \cdot (\boldsymbol{u}'C_{\text{eq}}) \rangle$.

Hence, the only contribution to the advective flux that results in a net bottom change is due to $u_{\text{eq}}C'$. To study this contribution, we consider the advective part $\hat{\mathscr{V}}_{\text{adv}}$ of the so-called total net advective volumetric sediment transport $\hat{\mathscr{V}}$ that leaves the region displayed in Fig. 2. The latter quantity is obtained by integrating the real part of Eq. (9) over region $\mathscr{D}$ and applying Gauss' law so that

$$\begin{aligned}\int_{\mathscr{D}} \Re\{h_{\text{t}}'\}\,\mathrm{d}^3x &= -\int_{\mathscr{D}} \Re\{\nabla \cdot \mathscr{F}\}\,\mathrm{d}^3x \\ &= -\int_{\partial\mathscr{D}} \Re\{\mathscr{F}\} \cdot \hat{\boldsymbol{n}}, \equiv -\hat{\mathscr{V}},\end{aligned} \tag{15}$$

where $\partial\mathscr{D}$ and $\hat{\boldsymbol{n}}$ denote the boundary of domain $\mathscr{D}$ and its outward directed unit normal vector, respectively. The resulting expressing for $\hat{\mathscr{V}}$ can be written as

$$\hat{\mathscr{V}} = \hat{\mathscr{V}}_{\text{adv}} + \hat{\mathscr{V}}_{\text{diff}} + \hat{\mathscr{V}}_{\text{bed}}$$

with

$$\hat{\mathscr{V}}_{\text{adv}} = \frac{2}{l_n}\Re\{\mathrm{i}\langle u_{\text{eq}}(t)\hat{C}(t)\rangle\}. \tag{16}$$

Ignoring sediment dispersion and bedslope effects, one can use Eqs. (9), (12), (15) and the fact that $\hat{h}$ is real to find that the advective volumetric transport is related to the growth rate by $\hat{\mathscr{V}}_{\text{adv}} \equiv \hat{\mathscr{V}} = -2\omega\hat{h}/(kl_n)$. Thus, we find advective processes to give growth/decay of the crest inside the enclosed region if there is a net import/export by advection, which corresponds to negative/positive $\hat{\mathscr{V}}_{\text{adv}}$. Consequently, positive and negative values for $\hat{\mathscr{V}}_{\text{adv}}$ will indicate whether sediment advection will contribute to decay or growth of bedforms, respectively.

4. Results

In this section results from the local 2D channel model will be described. Default values which are

characteristic for the Western Scheldt will be used, see Table 1. The growth rates presented below will be expressed in units $\alpha U^2/H$, where $U \equiv 1$ m s^{-1}, while k is scaled in units of the tidal excursion length $\ell = U/\sigma$. Hence, the scaled growth rate $\omega = 1$ corresponds to a dimensional e-folding timescale of 2 weeks for fine sand and to 3 years for medium sand. The scaled longitudinal wavenumber $k = 1$ corresponds to a dimensional wavelength of approximately 7 km. In the remainder of this paper, we will only consider advective modes, i.e. horizontal dispersion terms in the momentum and concentration equations are neglected ($\mu = 0$). This is justified since the ratio of dispersive to advective fluxes is of the order 10^{-1}–10^{-3} for the bed form length scales that are considered in this paper. This is also done in the model adopted by Seminara and Tubino (1998).

4.1. Advective instabilities for linear bottom friction

First, the growth of advective bed forms will be discussed in the absence of bed slope effects ($\lambda = 0$).

Fig. 3 shows the dimensionless growth rate as a function of the dimensionless longitudinal wavenumber k for various values of the lateral number n. We see that all curves are marginally stable for $k = 0$, as can be inferred from combining Eqs. (13) and (14) for $\mu = 0$ and $\lambda = 0$. Modes characterized by larger (but still moderate) k obtain positive growth rates while they eventually stabilize for sufficiently large longitudinal wavenumber.

Table 1
Parameter values, representative for the marine part of the Western Scheldt

Variable	Symbol	Repr. value
Water depth	H	10 m
Embayment width	B	5×10^3 m
Tidal frequency	σ	1.4×10^{-4} s^{-1}
Velocity scale	U	1 m s^{-1}
Settling parameter	γ	8×10^{-3} s^{-1}
Friction parameter	r	10^{-3} m s^{-1}
Erosion constant	α	10^{-5}–10^{-7} s m^{-1}
Bedslope parameter	λ	10^{-2}–10^{-4} m^2 s^{-1}

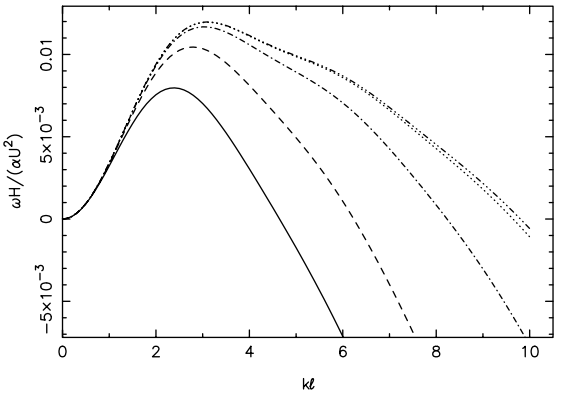

Fig. 3. Non-dimensional growth rate ω versus non-dimensional longitudinal wavenumber k for $n = 1$ (—), $n = 5$ (– – –), $n = 20$ (– · –), $n = 100$ (· · · · ·) and $n = 100\,000$ (– · · · –).

It is found that the maximum growth rate for a given longitudinal wavenumber increases monotonically with n. Moreover, there appears to be a limiting curve $\omega_\infty(k)$ to which $\omega(k)$ converges from below as $n \to \infty$. Thus, the preferred mode of bottom growth corresponds to a finite longitudinal wavenumber k but it has infinite lateral wavenumber, i.e. the preferred mode is a *braiding* mode at about $k\ell = 3$ which corresponds to a wavelength of approximately $2\ell \approx 14$ km. This result is reminiscent from river morphodynamics where this mode is also found to be the most unstable one if bed slope effects are neglected (Callander, 1969).

To understand the physical mechanism responsible for the instability observed for long-wave perturbations (k small) and the stabilizing physical effect when k is increased, we again consider the volumetric outward-directed transport $\hat{\mathscr{V}}$ from the region in Fig. 2 that encloses a crest. Moreover, as we ignore both diffusion and bedslope effects in this subsection, we have $\hat{\mathscr{V}} \equiv \hat{\mathscr{V}}_{\text{adv}}$.

The physics behind growth and decay of bed forms is most clearly identified by considering the limits of very long and very short wavelength perturbations for a fixed lateral modenumber n. For long waves, sediment transport is mainly driven by the residual velocity perturbation $\langle u' \rangle$. This rectified velocity component is generated by

tide-topography interaction that originates from bottom friction. It sets up a net sediment flux towards crests which results in growth of bed forms. On the other hand, the dynamics of sediment transport for short wavelength perturbations are entirely determined by the M_2 component of u' that follows from mass conservation. This will generate a net sediment flux from crests to troughs. These features will now be explained in more detail.

For long-wave perturbations (k small), the sediment dynamics can be approximated by a balance between erosion and deposition (right-hand side of Eq. (8d)), i.e. $C' \approx 2u_{eq}u'$. Hence, the total net outward-directed volumetric sediment transport $\hat{\mathscr{V}}$ from the fundamental domain in Fig. 2 reads

$$\hat{\mathscr{V}} = \frac{2}{l_n}\Re\{\mathrm{i}\langle u_{eq}\hat{C}\rangle\} = 4\frac{\alpha}{l_n\gamma}\Re\{\mathrm{i}\langle u_{eq}^2\hat{u}\rangle\}$$
$$= 2\frac{\alpha U^2}{l_n\gamma}\Re\{\mathrm{i}\langle\hat{u}\rangle\}, \qquad (17)$$

where we have used $\langle u_{eq}^2\rangle = U^2/2$ and neglected the M_4 component of the perturbed along-channel velocity u' since it is usually smaller than the residual. Expression (17) shows that the growth of long-wave perturbations is primarily governed by the residual perturbed velocity $\langle u'\rangle$. Fig. 4 shows a typical example of the behaviour of this quantity as the longitudinal wavenumber k varies. From this plot it is found that $\Im\langle u'\rangle$ is always positive and, using Eq. (17), a net sediment transport into the region is found. This is a destabilizing effect as it leads to net deposition inside the region. From Fig. 4 we also see, that the magnitude of $\Im\langle u'\rangle$ reaches a maximum at $k\ell = O(1)$; this determines the position of the maximum of the growth curve in Fig. 3.

In case of short wave perturbations (k large), the advective contributions to the sediment concentration equation (8d) cannot be neglected anymore. Combining Eqs. (8d), (10a) and (14) with $\mu = 0$ one finds that the perturbed sediment concentration for $k \gg 1$ approximately reads

$$\hat{C} = -C_{eq}\frac{\hat{h}}{H} - \frac{\mathrm{i}\alpha}{k}\left[2\hat{u} + u_{eq}\frac{\hat{h}}{H}\right], \qquad (18)$$

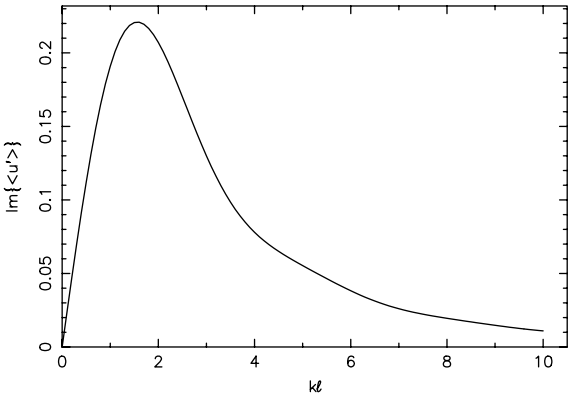

Fig. 4. Amplitude $\langle\hat{u}\rangle$ of the along-channel perturbed residual velocity $\langle u'\rangle$ versus dimensionless longitudinal wavenumber. The scaling along the vertical axis is in units $U\hat{h}/H$ m s^{-1}. This result refers to $n = 1$ and $B = 5$ km. The spatial variation of the residual current $\langle u'\rangle$ for a fixed longitudinal wavenumber k is obtained by multiplying the value of $\langle\hat{u}\rangle$ at a fixed value of k with its corresponding spatial eigenvalue structure, obtained from (10).

so that the outward-directed transport $\hat{\mathscr{V}}$ leaving the fundamental domain is given by

$$\hat{\mathscr{V}} = \frac{2}{l_n}\Re\{\mathrm{i}\langle u_{eq}\hat{C}\rangle\}$$
$$= \frac{2\alpha}{l_n k}\left\langle 2u_{eq}\Re\{\hat{u}\} + u_{eq}^2\frac{\hat{h}}{H}\right\rangle. \qquad (19)$$

The first term indicates that the possible growth of the bottom is partly determined by the M_2 component of the perturbed velocity u'. To lowest order in k^{-1}, the residual velocity $\langle u'\rangle$ does not result in a net sediment transport. Using mass conservation (8a), it is found that above short wave bottom perturbations $u' \approx u_{eq}h'/H$, i.e. velocities are increased (decreased) above crests (troughs). As a result, the contribution $\propto u_{eq}u'$ is stabilizing since it yields a positive (i.e. outward directed) transport $\hat{\mathscr{V}}$ from a region enclosing a crest. The second contribution to Eq. (19) is always stabilizing since it is positive (i.e. directed out of the domain) for a region enclosing a crest ($\hat{h} > 0$), thus acting as a means to *erode* the crest. Therefore, short wave perturbations are found to be stable.

Finally, we note that it is shown in the appendix that the perturbed along-channel velocity u' becomes independent of lateral modenumber if n becomes large. In view of the above discussion, it

is then to be expected that the growth curve should approach a limit curve $\omega_\infty(k)$ as n increases, as is seen in Fig. 3.

4.2. Bedslope effects

Fig. 5 shows the same results as Fig. 3 but now with the effect of bedslope included; the adopted value for the slope parameter λ was 10^{-4} m^{-2} s^{-1}. As is to be expected, bedslope effects stabilize high n-modes. Consequently, the most unstable mode now occurs for finite n. Thus, the inclusion of bedslope effects results in *mode selection*, i.e. a mode with a low longitudinal and lateral wavenumber will generate the dominant spatial and temporal variation. Eigenfunctions with high modenumber n (i.e. fast spatial oscillations in the lateral direction) are damped. This is consistent with observations which indicate the absence of tidally driven bottom patterns at very small length scales.

Fig. 6 shows the neutral curves for the abovementioned bedslope parameter λ. A neutral curve $r_n(k)$ is defined as the relation between friction parameter r and wavenumber k for which the growth rate ω vanishes at a fixed lateral wavenumber n. This means that the amplitudes of the perturbations characterized by $(k, n, r_n(k))$ do not change in time. For friction values above the neutral curve, bedforms have positive growth rates. For r-values below the curve, the perturbations have negative growth rates, i.e. they are damped. The minimum of the neutral curve is referred to as the critical mode for the specified lateral modenumber n and is characterized by the critical wavenumber k_{cr} and friction parameter values r_{cr}. The critical mode marks the transition from decay of bedforms ($r < r_{cr}$) to growth of specific perturbations ($r > r_{cr}$).

The existence of a minimum for the neutral curves may be understood as follows. Bedslope effects yield a negative (i.e. stabilizing) contribution $-\lambda(k^2 + l_n^2)$ to the growth rate ω (see Eq. (13)). Hence, the destabilizing effect of bottom friction must be sufficiently strong to have bedforms with positive growth rates. Since this destabilizing effect has its maximum value for a finite value of k (see Fig. 3), it is to be expected that both r_{cr} and k_{cr} have finite (non-zero) values.

The curves in Fig. 6 show that the $n = 1$ mode is the first one to grow as r is increased from zero, followed subsequently by $n = 2, 3, \ldots$ etc. The critical wavenumbers $k_{cr,n}$ increase with n, see Table 2 for the first few modes. We thus find that the critical mode occurs at $n = 1$ so that the most unstable mode corresponds to a so-called *alternating bar* bedform.

4.3. Non-linear friction and the influence of channel width

In this section, we will extend our model by including non-linear bottom friction, which means

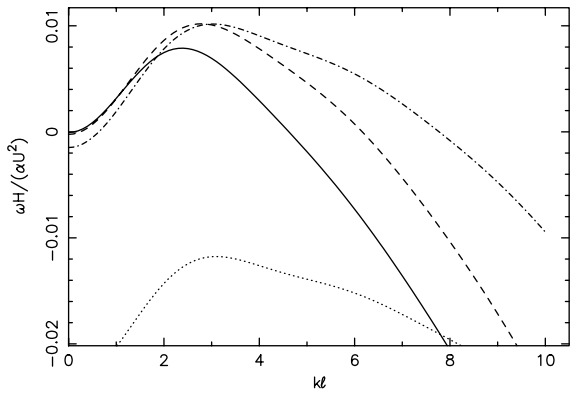

Fig. 5. Non-dimensional growth rate ω versus non-dimensional longitudinal wavenumber k for lateral wavenumber $n = 1$ (—), $n = 2$ (- - -), $n = 5$ (–·–), and $n = 20$ (· · · · ·). The $n = 100$ mode is so strongly damped that it lies below the lower limit of the panel.

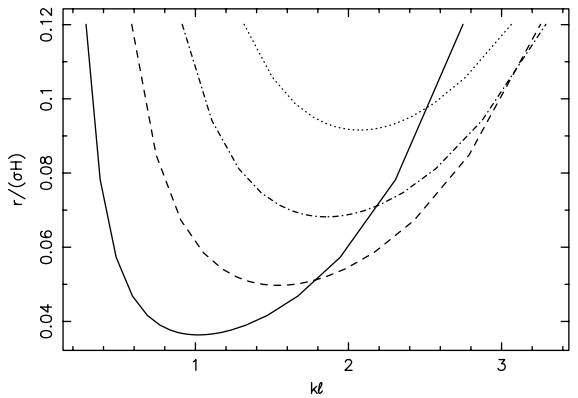

Fig. 6. Neutral curves for lateral wavenumbers $n = 1$ (—) $n = 2$ (- - -), $n = 3$ (–·–) and $n = 4$ (· · · · ·).

Table 2
Critical values of non-dimensional longitudinal wavenumber k and friction r for the first five unstable lateral mode numbers. Here $B = 5$ km and $\ell = 7$ km

n	$k_{cr}\ell$	$r_{cr}/(\sigma H)$
1	1.02	0.036
2	1.54	0.050
3	1.86	0.068
4	2.07	0.092
5	2.23	0.120

that $\boldsymbol{\tau}^b$ in Eq. (2) reads

$$\boldsymbol{\tau}^b = \rho \hat{r} \|\boldsymbol{u}\| \boldsymbol{u}, \tag{20}$$

where $\hat{r} = 3\pi r/(8U)$ follows from the Lorentz linearization procedure that was mentioned below Eq. (2). The effect of non-linearity on the growth of bedforms can be inferred from Fig. 7 which shows the neutral curves for both linear and non-linear friction. We see that the effect of non-linearity is to increase the threshold for instability as the critical friction parameter value is increased. Also, the most unstable wavenumber shifts towards a higher value, i.e. the critical mode occurs on a shorter longitudinal length scale.

The increase of the threshold for instability can be understood qualitatively as follows. As is explained in the appendix, the perturbed residual along-channel velocity $\langle u' \rangle$ may be inferred from the residual part of the perturbed vorticity $\Omega' = v'_x - u'_y$ as

$$\langle u' \rangle = \frac{l_n}{k^2 + l_n^2} \langle \Omega' \rangle.$$

The perturbed vorticity is created by a frictional torque. For linear friction, this torque is entirely due to the depth dependence of bottom stress which yields higher (lower) bottom friction above shallower (deeper) parts of the channel. For non-linear friction this torque is modified because the friction parameter $\hat{r}\|\boldsymbol{u}\|$ now depends upon velocity. Moreover, at values of the longitudinal wavenumber k where $\Im\langle u' \rangle$ reaches its maximum (see Fig. 4), frictional effects are important so that the tidal velocities are higher (lower) above troughs (crests). The explicit dependence of the non-linear friction parameter $\hat{r}\|\boldsymbol{u}\|$ on velocity thus yields a decrease (increase) of bottom friction above shallow (deep) parts of the channel. This results in a weakening of the frictional torque in comparison to the case of linear friction. Hence, the maximum value for $\Im\langle u' \rangle$ is expected to be lower for non-linear friction so that higher values for $\hat{r}$ are needed to surpass the threshold for growth of bedforms.

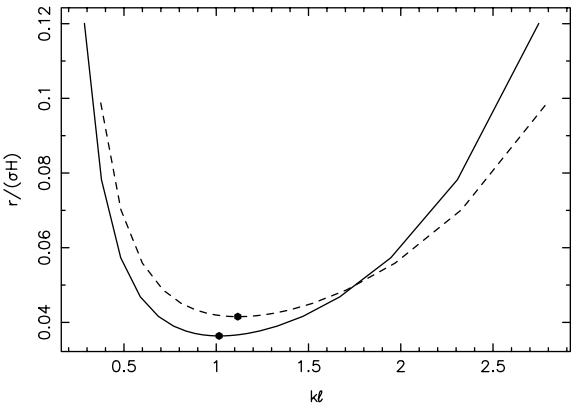

Fig. 7. Neutral curves for the alternating bar ($n = 1$) mode for a wide channel ($B = 5$ km). The solid and dashed lines refer to linear and non-linear friction, respectively, while the critical modes have been marked by dots.

Next, we investigate the effect of variation in channel width. So far, we have considered a so-called wide channel for which width and tidal excursion length are of the same order of magnitude. This means that the ratio ε of inertia (magnitude $\approx \sigma U$) to advective processes (magnitude $\approx U^2/B$)

$$\varepsilon = \frac{\sigma B}{U} = \frac{B}{\ell} \tag{21}$$

is of order unity. We now turn to the case of a narrow channel, for which $B \ll \ell$ (i.e. $\varepsilon \ll 1$). If, additionally, such a channel is frictionally dominated in the sense that the bottom friction term (magnitude $\approx rU/H$) is large compared to the inertial term (i.e. $r/(\sigma H) \gg 1$) the explicit time dependence of fluid velocity is negligible. The latter approximation was adopted by Seminara and Tubino (1998). Note that neither their results nor the present ones refer to a frictionally dominated situation since in both cases, the critical mode occurs at $r_{cr} \ll \sigma H$. The effect of inertia will now be investigated explicitly by considering growth of bedforms in a narrow channel of width $B = 500$ m ($\varepsilon = 0.07$).

Figs. 8 and 9 show the effect of small but finite ε in case of linear and non-linear friction, respectively. In both figures, two curves are plotted: one for $\varepsilon = 0$ (inertia ignored) and one for the small but finite ε ($\varepsilon = 0.07$) that corresponds to $B =$ 500 m. For both linear and non-linear bottom friction, we find that incorporation of small but finite inertia yields a shift of the critical wavenumber to higher values, i.e. the critical bedform shifts towards smaller length scales. Hence, it appears that neglecting explicit time variations of fluid velocity for narrow, non-frictionally dominated channels will *overestimate* the length scale of bottom patterns.

We note that the critical friction parameter values are much higher than for the wide channel ($B = 5$ km), see Fig. 7. This is because for a fixed lateral wavenumber n, the lateral bottom variations are steeper if the width is smaller; this enhances the stabilizing effect of bedslopes. The destabilizing effect of friction, on the other hand, becomes constant for narrow channels (see the appendix). This results in a higher friction value that is required to trigger instability.

Also, we observe from Figs. 8 and 9 that the qualitative differences between linear and non-linear friction in Fig. 7 remain unaltered for either $\varepsilon = 0$ or $\varepsilon = 0.07$. Hence, also for narrow channels we find that the effect of non-linear friction is to increase the threshold r_{cr} for instability as well as

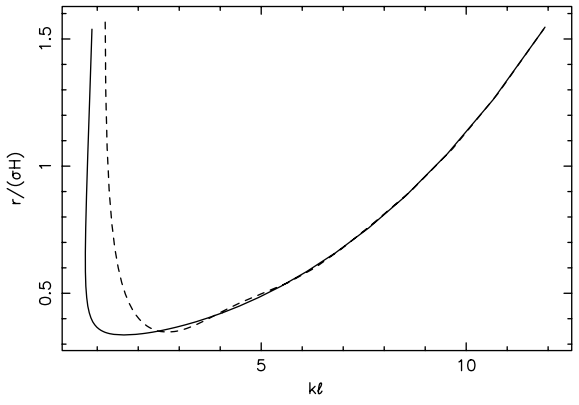

Fig. 8. Neutral curves for lateral modenumber $n = 1$ for a narrow channel ($B = 500$ m) with linear friction. The solid and dashed curves refer to $\varepsilon = 0$ (inertia ignored) and $\varepsilon = 0.07$, respectively. To scale k with the width, one can multiply these values by a factor $B/\ell = 0.07$.

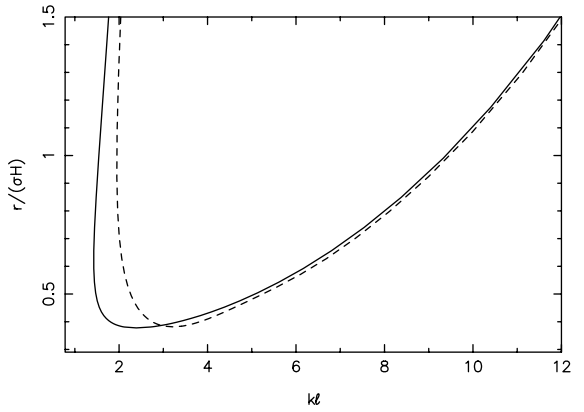

Fig. 9. Neutral curves for lateral modenumber $n = 1$ for a narrow channel ($B = 500$ m) with non-linear friction. The solid and dashed curves refer to $\varepsilon = 0$ (inertia ignored) and $\varepsilon = 0.07$, respectively. To scale k with the width, one can multiply these values by a factor $B/\ell = 0.07$.

the longitudinal wavenumber k_{cr} of the critical mode. Finally, we will compare the results for non-linear friction and $\varepsilon = 0$ (solid line in Fig. 9) to results of Seminara and Tubino (1998), since this specific case is the 2D-counterpart of their 3D model. The qualitative shape of the neutral curve for non-linear friction (e.g. multivaluedness for smaller k-values, which implies that long-wavelength bottom perturbations always decay) is similar to the findings of Seminara and Tubino (1998). Quantitatively, the value of the critical wavenumber in our case is approximately $k_{cr}B =$ 0.17. This compares well with the values obtained by Seminara and Tubino (1998), who found $k_{cr}B$ to lie in the range 0.1–0.5. However, the relationship that the critical wavenumber $k_{cr,n}$ of mode n obeys $k_{cr,n} = nk_{cr,1}$ has not been reproduced.

5. Discussion and conclusions

In this paper, the formation of bottom patterns that scale with the tidal excursion length has been studied within a 2D idealized model. Within the model, bathymetric features can arise as an inherent instability due to the interaction between water motion and sediment transport. In the case that sediment diffusion can be neglected, this instability is mediated by advective processes, in

particular through residual flows that arise from tide-topography interactions. In particular, such flows always set up net sediment fluxes towards shoals and away from deep channels. For longitudinal small-scale bedforms (along-channel dimensions well below one tidal excursion length), the M_2 part of the topographically induced flow determines the net sediment fluxes. These fluxes always turn out to be stabilizing, i.e. they counteract formation of longitudinal small-scale bottom patterns.

Bed slope effects act as a means to prevent the emergence of both longitudinal and lateral small-scale features. Moreover, they cause *mode selection* which enables a low-order lateral mode to occur most easily: for a realistic bedslope parameter $\lambda = 10^{-4}$ m^2 s^{-1}, this is the alternating bar or $n = 1$ mode. This can be illuminated by the use of neutral curves, which predict threshold values for the friction parameter which must be exceeded in order to enable growth of the most unstable bedform. It turns out that the most unstable modes occur on a length scale that is comparable to the tidal excursion length, independent of either the width of the embayment or the adopted parameterization for bottom friction (i.e. linear or non-linear).

The neutral curves obtained in the 2D model show good qualitative agreement with the findings of Seminara and Tubino (1998), in particular if a non-linear formulation for bed shear stress is adopted. On the other hand, there are distinct differences. For instance, it appears that explicit time dependence of water motion (fluid inertia) may have a significant effect on the length scale of the critical bottom mode (see Fig. 9), even if the channel is narrow (i.e. $B \ll \ell$). This discrepancy seems to be robust as it is also found if linear bottom friction is adopted (see Fig. 8). We attribute this effect to the fact that fluid inertia is not negligible under circumstances which are not frictionally dominated: this is the case here since the most unstable critical bottom mode occurs at $r_{cr} \ll \sigma H$.

Nonetheless, the qualitative agreement between the present model and Seminara and Tubino (1998) is remarkable if one takes into account the considerable differences in model formulations. These differences include, among others, 2D versus 3D prescription and a different formulation for erosion–deposition rates. All these discrepancies may in principle yield qualitatively different outcome. Apparently, the physical mechanism that governs the formation of bedforms is relatively insensitive to the details of such formulations.

Acknowledgements

This research was supported by the National Institute for Coastal and Marine Management at The Hague, The Netherlands, and by the Council of Earth and Life Sciences (ALW) of the Dutch National Science Foundation (NWO).

Appendix. Perturbed vorticity equation and perturbed flow

Below, we will elaborate on the relationship between perturbed along-channel velocity u' and the perturbed vorticity $\Omega' \equiv v'_x - u'_y$. The time evolution of the latter quantity can be found by differentiating Eqs. (8b) and (8c) by y and x, respectively, and subtracting the results. Using Eq. (10) one arrives at

$$\hat{\Omega}_t + \mathrm{i}ku_{\mathrm{eq}}\hat{\Omega} + \frac{\hat{r}||\boldsymbol{u}_{\mathrm{eq}}||}{H}\hat{\Omega} = -\frac{\hat{r}||\boldsymbol{u}_{\mathrm{eq}}||l_n}{H}\left[u_{\mathrm{eq}}\frac{\hat{h}}{H} + \hat{u}\right] \tag{A.1}$$

with $\hat{\Omega}$ being given by definition by

$$\hat{\Omega} \equiv \mathrm{i}k\hat{v} + l_n\hat{u}. \tag{A.2}$$

In Eq. (A.1), the non-linear bottom stress parameterization has been adopted. The result for linear friction is obtained by replacing $\hat{r}||\boldsymbol{u}_{\mathrm{eq}}||$ by r and omitting the second term in the square brackets in Eq. (A.1). The two terms between these brackets represent the tidal torques that are due to the depth dependence of bottom stress and velocity dependence of the non-linear friction parameter $\hat{r}||\boldsymbol{u}||$, respectively.

Similarly, the perturbed part of mass conservation (8a) can be written as

$$\mathrm{i}k\hat{u} + l_n\hat{v} = \mathrm{i}ku_{\mathrm{eq}}\frac{\hat{h}}{H}. \tag{A.3}$$

If the perturbed vorticity is known, the along-channel velocity $\hat{u}$ is found from Eqs. (A.2) and (A.3) and reads

$$\hat{u} = \frac{1}{k^2 + l_n^2}\left[l_n\hat{\Omega} + k^2 u_{\mathrm{eq}}\frac{\hat{h}}{H}\right]. \tag{A.4}$$

Finally, we consider the limit $l_n\ell = n\pi\ell/B \gg 1$. Note that this encompasses both the case of high lateral modenumber n as well as a narrow channel. From mass conservation we find that $\hat{v}/\hat{u} \sim l_n^{-1}$ so that $\hat{\Omega} \approx l_n\hat{u}$. This implies that the vorticity equation (A.1) reduces to

$$\hat{u}_t + \mathrm{i}ku_{\mathrm{eq}}\hat{u} + \frac{\hat{r}||u_{\mathrm{eq}}||}{H}\hat{u} = -\frac{\hat{r}||\boldsymbol{u}_{\mathrm{eq}}||}{H}\left[u_{\mathrm{eq}}\frac{\hat{h}}{H} + \hat{u}\right], \tag{A.5}$$

that is, the magnitude of the perturbed along-channel velocity $\hat{u}$ does not depend upon either lateral modenumber n or channel width B. Regarding the residual $\langle\hat{u}\rangle$ this result indicates that the strength of the destabilizing mechanism that underlies growth of bedforms will become constant if $l_n\ell \gg 1$.

References

Callander, R., 1969. Instability and river channels. Journal of Fluid Mechanics 36, 465–480.

Cleveringa, J., Oost, A.P., 1999. The fractal geometry of tidal channel systems in the Dutch Wadden Sea. Geologie en Mijnbouw 78, 21–30 (special issue on prediction in Geology).

Dalrymple, R.W., Rhodes, R.M., 1995. Estuarine dunes and bars. In: Perillo, G.M.E. (Ed.), Geomorphology and Sedimentology of Estuaries, Development in Sedimentology, Vol. 53. Elsevier, New York, pp. 359–422.

Di Silvio, G., 1989. Modelling the morphological evolution of tidal lagoons and their equilibrium configurations. In: Proceedings of the XIIIrd IAHR Congress, IAHR.

Dyer, K.R., 1986. Coastal and Estuarine Sediment Dynamics. Wiley, Chichester.

Ehlers, J., 1988. The Morphodynamics of the Wadden Sea. Balkema, Rotterdam.

Engelund, F., 1975. Instability of flow in a curved alluvial channel. Journal of Fluid Mechanics 72, 145–160.

Hulscher, S.J.M.H., de Swart, H.E., De Vriend, H., 1993. The generation of offshore tidal sand banks and sand waves. Continental Shelf Research 13 (11), 1183–1204.

Jeuken, M.C.J.L., 2000. On the Morphologic Behaviour of Tidal Channels in the Westerschelde Estuary. Netherlands Geographical Studies, Vol. 279. KNAG, Utrecht.

Lorentz, H.A., 1922. Het in rekening brengen van den weerstand bij schommelende vloeistofbewegingen. De Ingenieur 37, 695–696.

Parker, G., 1978. Self-formed straight rivers with equilibrium banks and mobile bed. Part 1, the sand–silt river. Journal of Fluid Mechanics 89, 109–125.

Ranasinghe, R., Pattiaratchi, C., Masselink, G., 1999. A morphodynamic model to simulate the seasonal closure of tidal inlets. Coastal Engineering 37, 1–36.

Schuttelaars, H.M., De Swart, H.E., 1999. Initial formation of channels and shoals in a short tidal embayment. Journal of Fluid Mechanics 386, 15–42.

Schuttelaars, H.M., De Swart, H.E., 2000. Multiple morphodynamic equilibria in tidal embayments. Journal of Geophysics Research 105, 24,105–24,118.

Schuttelaars, H.M., Schramkowski, G.P., De Swart, H.E., 2001. Initial formation of estuarine sections. Proceedings of the 2nd IAHR Symposium on River, Coastal and Estuarine Morphodynamics (RCEM 2001), 10–14 September 2001, Obihiro, Japan, pp. 443–452.

Seminara, G., Tubino, M., 1998. On the formation of estuarine free bars. In: Dronkers, J., Scheffers, M. (Eds.), Physics of Estuaries and Coastal Seas, PECS 96. Balkema, Rotterdam.

Talmon, A.M., Van Mierlo, M.C.L.M., Struiksma, N., 1995. Laboratory measurements of the direction of sediment transport on transverse alluvial-bed slopes. Journal of Hydraulic Research 33, 495–517.

Van den Berg, J., Jeuken, M., van der Spek, A., 1997. Hydraulic processes affecting the morphology and evolution of Westerschelde estuary. In: Nordstrom, K., Roman, C. (Eds.), Estuarine Shores: Evolution, Environments and Human Alterations. Wiley, Chichester.

Van Dongeren, A.R., de Vriend, H.J., 1994. A model of morphological behaviour of tidal basins. Coastal Engineering 22, 287–310.

Van Leeuwen, S.M., De Swart, H.E., 2001. The effect of advective processes on the morphodynamic stability of short tidal embayments. Physical Chemistry of Earth (B) 26, 735–740.

Van Rijn, L.C., 1993. Principles of Sediment Transport in Rivers, Estuaries and Coastal Seas. Aqua Publications, Amsterdam.

Verbeek, H., Wang, Z., Thoolen, P., 1999. Secondary currents in estuarine morphodynamic modelling, a case-study of the western scheldt. Proceedings of the IAHR Symposium on River, Coastal and Estuarine Morphodynamics, 6–10 September 1999, Genova, Italy, pp. 649–658.

Vreugdenhil, 1994. Numerical Methods for Shallow Water Flow. Water Science & Technical Library, Kluwer, Norwell, MA.

Wang, Z., Louters, T., De Vriend, H., 1995. Morphodynamic modelling for a tidal inlet in the Wadden Sea. Marine Geology 126, 289–300.

Zimmerman, J.T.F., 1992. On the Lorentz linearization of a nonlinearly damped tidal Helmholtz oscillator. Proceedings, Koninklijke Nederlandse Akademie van Wetenschappen 95, 127–145.